



# High-detection-efficiency stereo microscope system based on a mobile phone

XINRAN GUO,<sup>1</sup> JUN CHANG,<sup>1,\*</sup> WEILIN CHEN,<sup>1</sup> YAoyao HU,<sup>1</sup>  NING MA,<sup>1</sup> AND JIANPING ZHANG<sup>2,3</sup>

<sup>1</sup>School of Optics and Photonics, Beijing Institute of Technology, Beijing 100081, China

<sup>2</sup>Changchun Institute of Optics, Fine Mechanics and Physics, Chinese Academy of Sciences, Beijing 100190, China

<sup>3</sup>Key Laboratory of Optical System Advanced Manufacturing Technology, Chinese Academy of Sciences, Changchun 130033, China

\*optics\_chang@126.com

Received 17 March 2023; revised 27 May 2023; accepted 30 May 2023; posted 30 May 2023; published 26 June 2023

**Most stereoscopic microscopes used for industrial component detection are large and have low detection efficiencies. The use of mobile phones as imaging systems (rather than conventional sensors) in industrial fields would make industrial testing more convenient. In this study, an external stereo microscope for mobile phones is designed. The proposed system can resolve details up to 0.01 mm with an 11 mm object field of view,  $-6.34\times$  angular magnification, and quantitative 3D feature measurement. The combined system proposed in this paper is suitable for the microscopic observation of industrial components, with its low cost, high detection efficiency, and short installation steps.** © 2023 Optica Publishing Group

<https://doi.org/10.1364/AO.489445>

## 1. INTRODUCTION

Integrated circuit (IC) packages represent the cutting edge of packaging technology. To achieve high-level integration, smaller electronic components have been developed [1,2]. Due to the increased density of electronic devices on a circuit board, measuring instruments that can quickly, accurately, and cost-effectively capture the shape, position, distance, and quantity of electronic devices are essential for industrial manufacturers.

Conventional microscopes for human eye observation, and digital stereo microscopes are commonly used for industrial observation [3,4]. However, these instruments need to be connected to a power supply and fixed on an optical platform to ensure imaging stability, which results in low detection efficiency of industrial microscopy. Apart from that, microscopes for human eye observation are limited in terms of 3D feature recovery due to the parallax effect based on the human eye not achieving accurate depth measurement.

In terms of high-precision 3D feature recovery technologies used in industry, structured light illumination is an active 3D scanning technique that uses a projector and camera pair to project and capture a series of stripe patterns [5–8]. However, the irregular arrangement of electronic chips with different heights on the circuit board causes obscuration, which further hinders the measurement. Confocal microscopes [9,10], near-field scanning optical microscopes [11], and white-light interference microscopy [12] have the capability to obtain 3D information with extreme precision. However, high demands on equipment, including accuracy and stability, make them difficult to be commercialized. 3D shape recovery from an image focus based

on liquid lenses and zoom objectives can achieve extended depth of field imaging, but multiple adjustments of the drive voltage would increase the shooting time [13,14].

Considering portability and detection efficiency, numerous generations of cellphone-based microscopes have been proposed and commercialized [15–22]. However, the lack of 3D recovery capability means these technologies cannot be used in industrial tests.

Therefore, a microscope system with a quantitative 3D feature measurement function and remarkable image quality is necessary for industrial testing. Cost effectiveness, high detection efficiency, and short shooting times are important factors as well that ensure the entire system can be commercialized.

In this study, an industrial stereomicroscope based on dual mobile phone cameras with light weight, remarkable image quality, and a quantitative 3D feature measurement function is proposed. Only lighting devices and mobile phones with clear imaging capability are required in the process of microscopic observation, which ensures its high adaptability. The proposed stereomicroscope is cost effective because the optical parts are composed of commercially available lenses. We verify the suitability of this system and prove that the technology enables general-purpose high-detection-efficiency microscopy. The proposed technology can be applied in industrial 3D inspection and is expected to fuel the development of IC packaging technology.

## 2. DESIGN METHOD OF THE STEREO MICROSCOPE BASED ON A CELLPHONE

Using HUAWEI MATE 20 as an example, this section describes the design and evaluation process of the stereomicroscope, including the optimization results of the objective and eyepiece. A prototype portable stereomicroscope system based on commercially available lenses is presented.

### A. Optical System Design Considerations

The HUAWEI MATE 20 mobile phone consists of three rear cameras (an ultrawide angle lens, wide angle lens, and 2× telephoto lens). These cameras can be invoked separately by adjusting the capture mode of the control panel. A wide angle lens and 2× telephoto lens are selected as the imaging systems at the end of the left and right light paths, respectively. This results in effective object distances ranging from 100 mm to infinity. The parameters of the HUAWEI MATE 20 built-in cameras are listed in Table 1 according to the information disclosed at the HUAWEI press conference [23].

The minimum component size of an industrial chip is approximately 0.01 mm. The numerical aperture of the microscope is calculated using the resolution limit formula [24,25].

$$\sigma = \frac{0.61\lambda}{\text{N.A.}}, \tag{1}$$

where  $\sigma$  is the minimum distance that the system can resolve,  $\lambda$  is the central wavelength, and N.A. is the numerical aperture of the objective. Considering the parameters of the mobile phone rear cameras and the minimum details that the entire system can resolve, the indicators of the proposed system are listed in Table 2.

**Table 1. Parameters of HUAWEI MATE 20 Rear Cameras**

Rear Camera	Resolution	F-Number	Equivalent Focal Length/mm
Wide angle lens	12 MP	1.8	27
2 × telephoto lens	8 MP	2.4	52

Rear Camera	Shooting Mode	D/mm	Actual Focal Length/mm
Wide angle lens	Standard	1.28	2.3
2 × telephoto lens	Large aperture	1.79	4.3

**Table 2. Optical System Indicators**

Indicators	Value
Wavelength	F, d, C (visible)
Entrance pupil diameter	12 mm
Field of view	11 mm
Angular magnification	−6.34×
Resolution	0.01 mm

Regarding the limited distance between dual mobile phone cameras, a stereo microscopy system was designed with a Galileo structure (see Fig. 1). The object was enlarged into a virtual image in front of the mobile phone through a secondary magnification of the objective and eyepiece. Then, the built-in cameras and mobile phone detectors captured the image. The entrance pupil of the entire system was located on the first surface of the objective, and the exit pupil was 6 mm behind the eyepiece. The built-in cameras of the cell phone, which are considered as paraxial systems, were located at the exit pupil of the entire system.

### B. Optical System Configuration

The microscope objective adopted a doublet as its initial structure. In the optimization steps, we mainly controlled the spherical, axial chromatic, and sinusoidal aberrations. The eyepiece has a short focal length and large field of view. It functions as secondary imaging equipment. The astigmatism and vertical-axis chromatic aberration should be corrected. After correcting the aberrations of the objective lens and eyepiece independently, aberration compensation should be considered by combining these. The total length of the system and magnification factor were considered as the optimal operands to ensure its limited volume and amplification effect. The optimization results were replaced with optical components available on the Daheng Optics online mall [26] (see Table 3).

The reflective prism and flat mirror in the beam splitting system were replaced by GPH11-010-VIS-02 (with a volume of 10 × 10 × 10 mm<sup>3</sup> and produced by the Hengyang Optical

**Table 3. Optical Components of the Stereo Microscopy System**

Serial Number (annotation)	Lens Model
1 (objective)	GCL-010603
2 (eyepiece 1)	GCL-010203
3 (eyepiece 2)	GCL-010169
4 (eyepiece 3)	GCL-010102

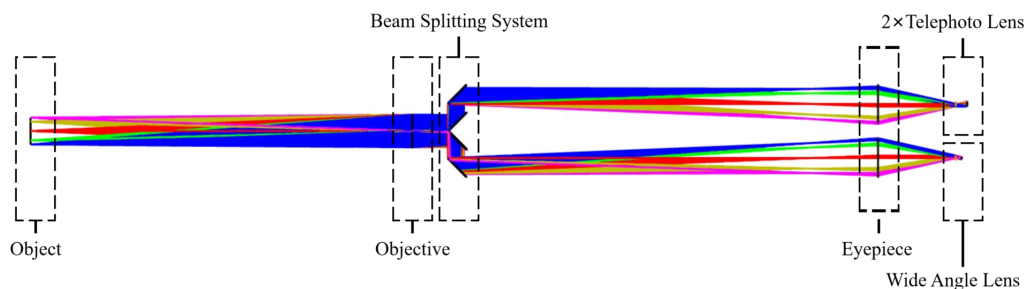


**Fig. 1.** Design scheme of stereo microscope based on mobile phone.

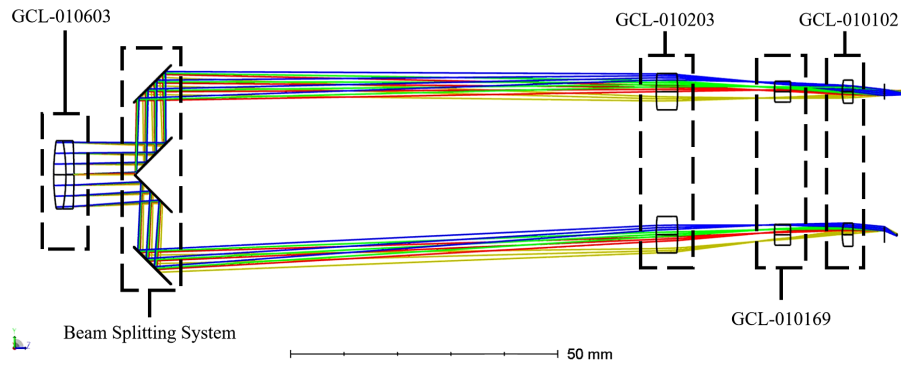


**Fig. 2.** Simulated light path of stereo microscope based on HUAWEI MATE 20.

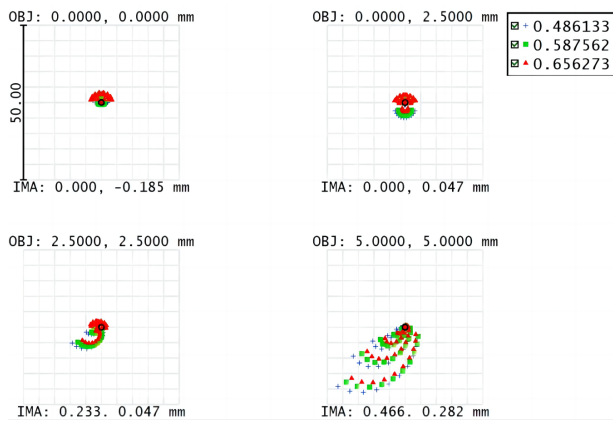


**Fig. 3.** Spot diagram for left light path (wide angle lens).

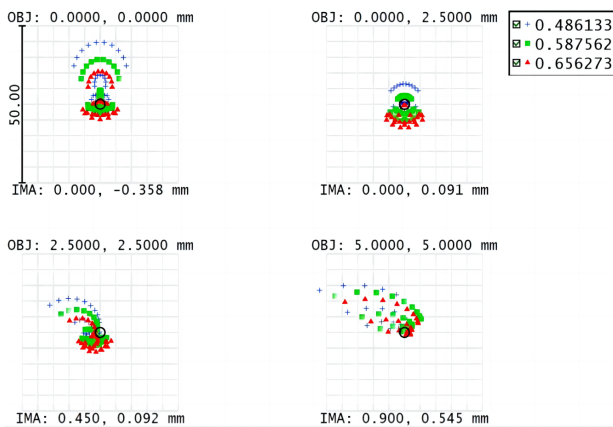


**Fig. 4.** Spot diagram for right light path (2× telephoto lens).

Company) [27] and GC-10226 with a 12.7 mm aperture and produced by Daheng Optics) [26], respectively. The simulated optical path of the system is illustrated in Fig. 2.

The spot diagram, modulation transfer function (MTF), and wave aberration map were selected as the comprehensive evaluation indices in the system because these reflect both diffraction limit resolution and aberration. The spot diagrams of the entire system in the image plane are shown in Figs. 3 and 4. The scale bar was measured in micrometers.

As an image quality evaluation criterion [28], the number of cycles per millimeter that the system can resolve is calculated

using Eq. (2):

$$\varepsilon_i = \varepsilon_o \times \Gamma, \quad (2)$$

where  $\varepsilon_i$  represents the minimum size that the system can resolve in the image plane.  $\varepsilon_o$  is the minimum size that can be distinguished in the object plane.  $\Gamma$  is the magnification of the optical system. For samples with a 0.01 mm minimum detail size, the MTF value at 278 cycles/mm for a wide angle lens and that at 139 cycles/mm for a 2× telephoto lens at the image plane were used as the criteria. The simulation results are shown in Figs. 5 and 6.

The wavefront maps for the two light paths are shown in Figs. 7 and 8. The root-mean-square wavefront aberrations of the two light paths were 0.2326 and 0.5134 waves, respectively. These are close to the Marechal criterion.

### C. Optical Mechanical Design

A half-sectional view of the stereomicroscope structure with mechanical support is shown in Fig. 9. The entire optical mechanical structure consists of four parts: objective fixing, mirror fixing, lens barrel, and eyepiece group fixing. The objective was locked through a peg, which was used to fix the position of the pressure ring in the lens cone. The reflecting prism and plane mirror in the beam splitting system were fixed using an optical adhesive. The eyepiece groups were separated by spacers and locked using a peg placed at the end of the system.

## 3. EXPERIMENTAL RESULTS

A top view of the left light path prototype of the system is shown in Fig. 10. The optical parts are composed of commercially available lenses. The specific models are listed in Table 3. The mechanical supports were printed using a Company Pro C300 dual-nozzle 3D printer with a printing accuracy of 1 mm and printing range of  $300 \times 300 \times 300 \text{ mm}^3$  [29]. In the experimental testing stage, we selected a white-light source to illuminate the circuit chip and used a three-screw laser tube holder to fix the entire system. The alignment of the optical axes between the objective and eyepiece groups was set by adjusting the six fixing screws.

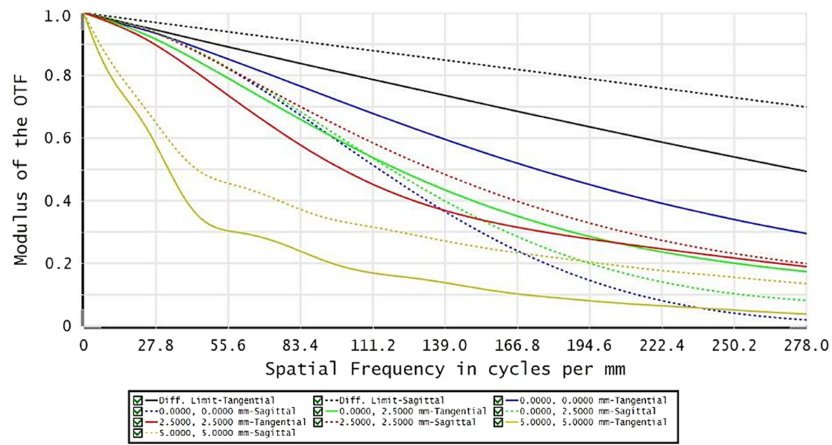


Fig. 5. MTF at 278 lp/mm for left light path (wide angle lens).

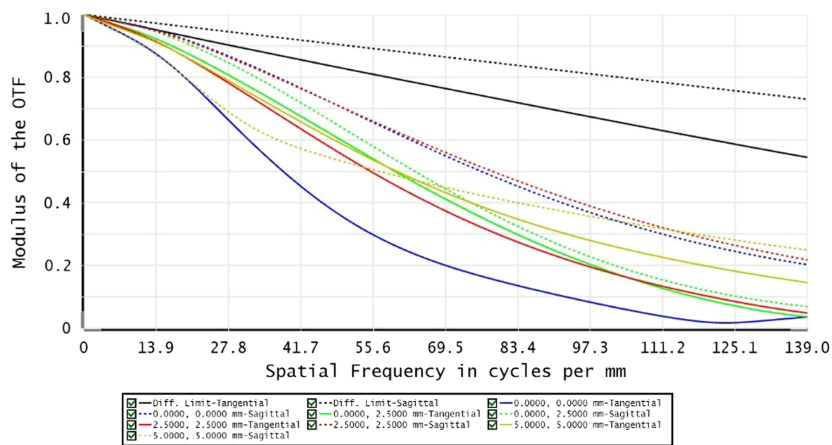


Fig. 6. MTF at 139 lp/mm for right light path (2x telephoto lens).

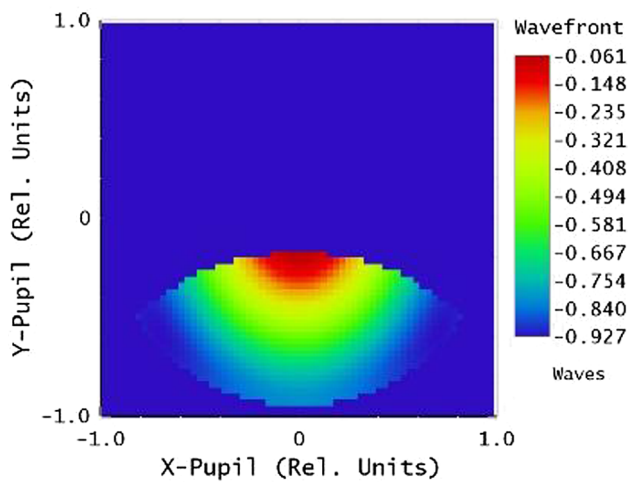


Fig. 7. Wavefront aberration for left light path (wide angle lens).

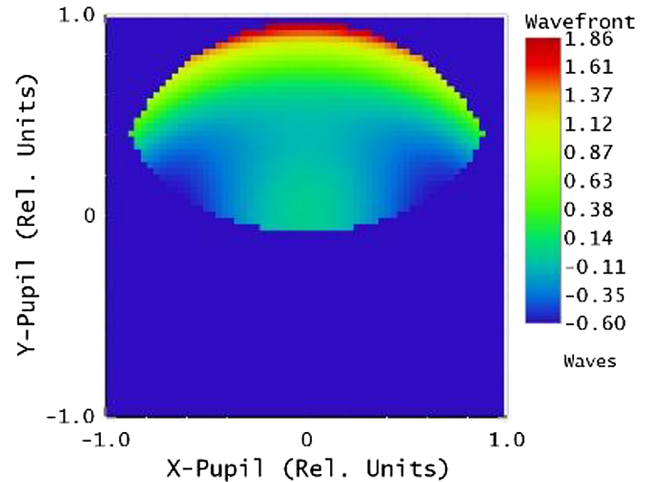
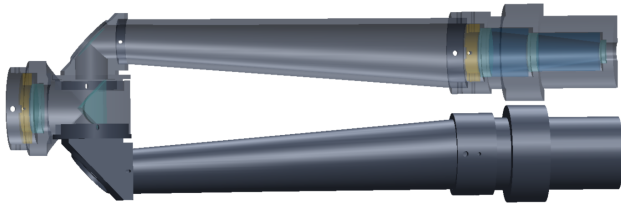


Fig. 8. Wavefront aberration for right light path (2x telephoto lens).

**A. Optical Resolution**

To analyze the resolving capability of the portable stereo microscopy system, we used the proposed system to photograph a GCG-020101 resolution board produced by Daheng

Optics [26]. With a working distance of 100 mm, the built-in mobile phone cameras could resolve details of approximately 0.025 mm. The resolution boards taken by the left and right



**Fig. 9.** Half-section view of the stereo microscope structure.

light paths are shown as images with black and red edges, respectively, in Fig. 11. The optical MTF curves of the corresponding light paths are shown as broken lines in Fig. 11. Compared with

using a mobile phone alone, the external stereo microscope improved the resolving capability by 2.5 times to 0.01 mm.

### B. Depth Information by Stereoscopic Vision

Figure 12 shows a photograph of the electronic chip captured only by the built-in cameras of the HUAWEI MATE 20. Here, details such as the electronic component model cannot be identified clearly. As shown in Figs. 13(a) and 13(b), the details in the white circle (Fig. 12) can be identified clearly by placing the stereo microscope in front of a wide angle lens and 2× telephoto lens, respectively.

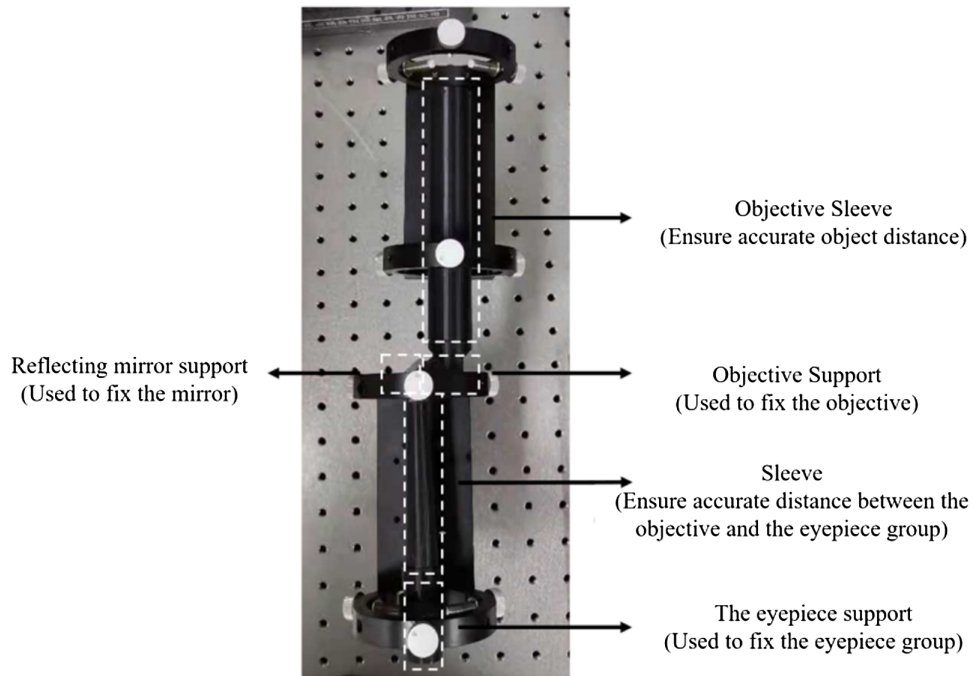


**Fig. 10.** Top view of the left light path testing structure.

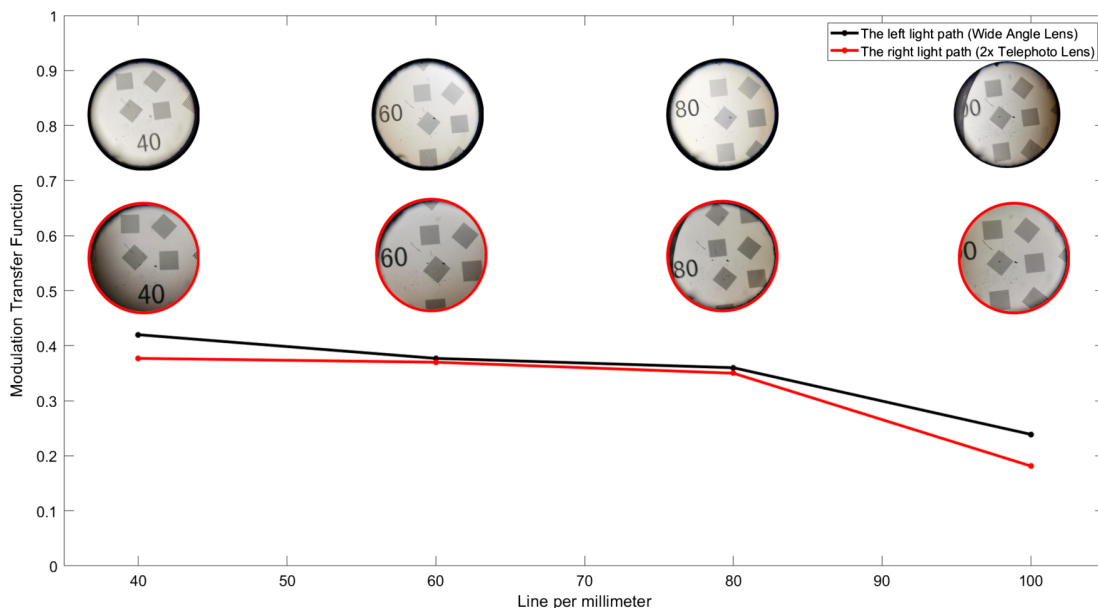


**Fig. 11.** Curves of modulation transfer function from 40 to 100 line/mm.

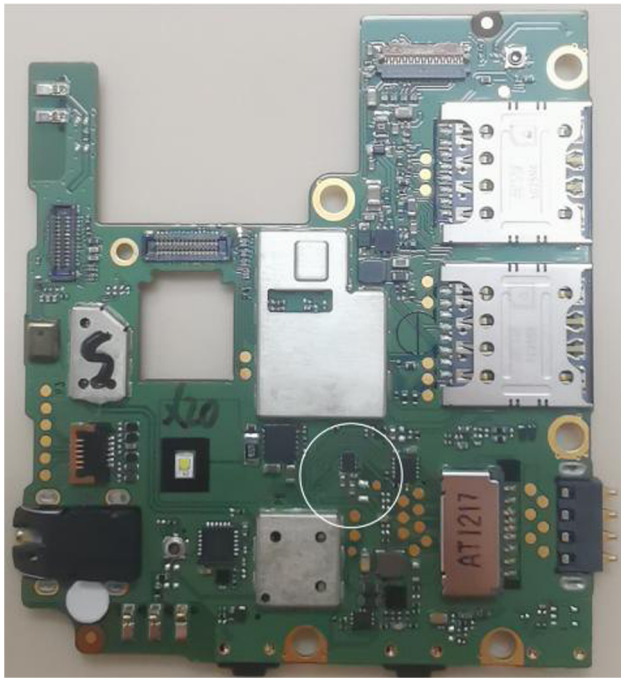


**Fig. 12.** Electronic chip photographed by the mobile phone built-in cameras only.

In addition, the proposed technology enables general-purpose high-detection-efficiency microscopy. We verified the suitability of this system. When the proposed system worked with an iPhone 12 built-in camera, it showed good experimental results (see Fig. 14).

When the front system is used to magnify the sample, the stereo vision capability of mobile phone binocular cameras improves. Stereo magnification is one of the parameters used to evaluate the 3D recovery capability. It is defined as the ratio between the optical parallax ( $\alpha_{\text{equipment}}$ ) observed by the proposed system and that ( $\alpha_{\text{rear camera}}$ ) observed by two mobile phone rear cameras only:

$$\Pi = \frac{\alpha_{\text{equipment}}}{\alpha_{\text{rear camera}}} = \frac{MP}{p}, \quad (3)$$

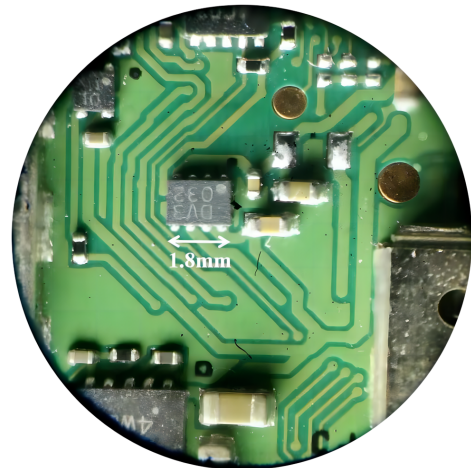
where  $M$  is the angular magnification of the microscope system.  $P$  and  $p$  indicate the entry pupil distance after the proposed system is added to the light path and that before this addition, respectively. The stereo magnification of the system was  $-6.34\times$ .

In the next step, we reconstructed the 3D shape of the circuit board using 3D reconstruction software [30,31]. The reconstruction results are shown in Fig. 15. The entire circuit board was located on approximately the same plane. Shadow bumps were observed on the DV3 032 chip. These were consistent with the chip bumps on the actual circuit board.

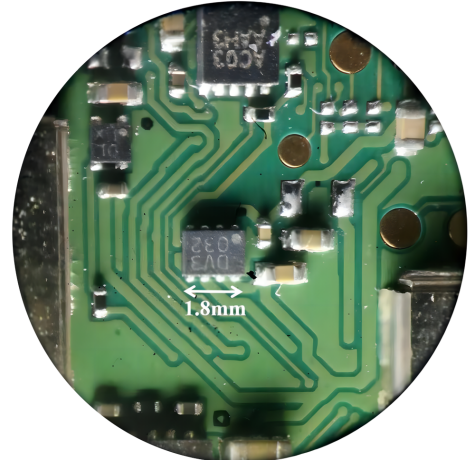
The reconstructed surface of the DV3 032 chip 3D model is shown in Fig. 16.

The average height of the DV3 032 chip was calculated as the ratio of  $\Delta z$  to  $\Delta x$ :

$$Z_{\text{average height}} = X_{\text{size}} \cdot \frac{\Delta z}{\Delta x}, \quad (4)$$



(a)



(b)

**Fig. 13.** Electronic chip photographed by the proposed system. (a) Left light path (wide angle lens light path) (b) Right light path ( $2\times$  telephoto lens light path).

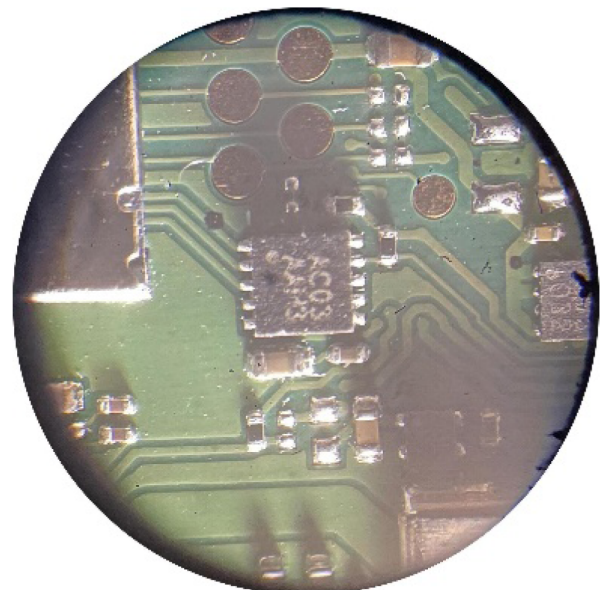


**Fig. 14.** Suitability verification for mobile phone model iPhone 12.

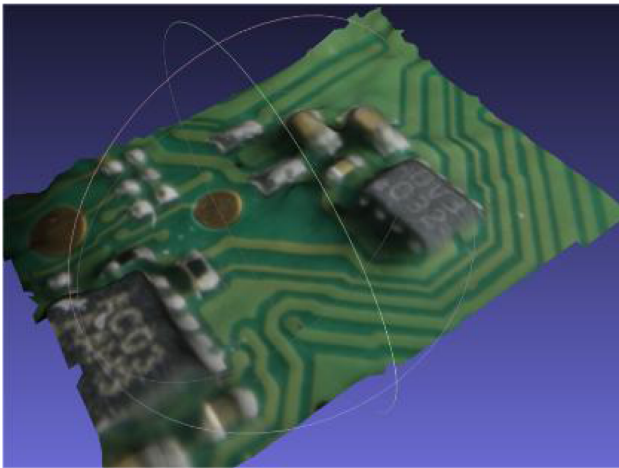


**Fig. 15.** 3D reconstruction result of the circuit board.

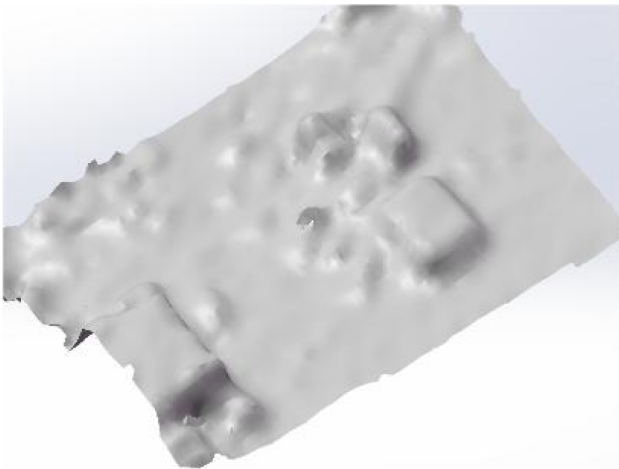


**Fig. 16.** Reconstructed surface of the DV3 032 chip.

where  $Z_{\text{average height}}$  indicates the real height of the DV3 032 chip and  $X_{\text{size}}$  is its length. The ratio of  $\Delta x$  to  $X_{\text{size}}$  represents the magnification of the entire optical system. By calculating Eq. (4), we estimated the real height of the DV3 032 chip to be approximately 0.45 mm. This is significantly close to 0.39 mm, which was the real height of the DV3 032 chip.

#### 4. DISCUSSION AND CONCLUSION

Based on the aberration theory, we propose a stereo microscopy prototype that can be matched with the dual cameras of mobile phones for photographing industrial chips.

The proposed stereomicroscope has advantages such as light weight, remarkable image quality, large magnification, low processing difficulty, and strong practicability compared with industrial microscopes available on the market (see Table 4) [26,32,33].

Compared with high-precision 3D feature recovery technologies such as confocal microscopes [9,10], near-field scanning optical microscopes [11], and white-light interference microscopy [12], the proposed system can realize the 3D feature recovery of complex surfaces inexpensively and with few operating procedures.

Compared with recently designed cellphone-based microscopes [17–20], the proposed system can achieve quantitative 3D feature measurement of complex surfaces with small sizes and depths (generally less than 1 mm). Apart from that, the proposed system can be adapted in most industrial observation scenarios because few specialized accessories are required in the optical path and can be fabricated by most optical and mechanical manufacturers because the tolerances of the system need not be controlled stringently.

The prototype can be combined with the rear lenses of most mobile phones available on the market to capture photographs. It is suitable for the observation and 3D reconstruction of electronic circuit boards and other devices in the industry. This is likely to improve the efficiency of the quality inspection and component selection procedures of the corresponding devices.

**Funding.** Key Laboratory of Optical System Advanced Manufacturing Technology, Chinese Academy of Sciences (2022KLOMT02-01).

**Acknowledgment.** The authors thank the anonymous reviewers for their valuable suggestions.

**Disclosures.** The authors declare no conflicts of interest.

**Data availability.** No data were generated or analyzed in the presented research.

#### REFERENCES

1. P. Aryan, S. Sampath, and H. Sohn, "An overview of non-destructive testing methods for integrated circuit packaging inspection," *Sensors* **18**, 1981 (2018).

**Table 4.** Technical Comparisons with Industrial Microscopes

Manufacturer	Model Number	Resolution	Optical Magnification	Field of View
Phenix [32]	XTL-165-LCD	0.0125 mm	0.6×	8 × 4.5 mm <sup>2</sup>
Daheng imaging [26]	TEC-V7X	0.024 mm	0.5×	24 × 24 mm <sup>2</sup>
Computar [33]	MLM-3XMP	0.0075 mm	1×	8.8 × 6.6 mm <sup>2</sup>
<b>Proposed system</b>		<b>0.01 mm</b>	<b>1.5×</b>	<b>11 × 11 mm</b>
Manufacturer	Model Number	Working Distance	Volume	Weight
Phenix [32]	XTL-165-LCD	100 mm	321 × 261 × 550 mm <sup>3</sup>	–
Daheng imaging [26]	TEC-V7X	182 mm	61 × 61 × 152.86 mm <sup>3</sup>	1400 g
Computar [33]	MLM-3XMP	90 mm	36.5 × 36.5 × 79.5 mm <sup>3</sup>	200 g
<b>Proposed system</b>		<b>142 mm</b>	<b>43 × 43 × 150 mm<sup>3</sup></b>	<b>50 g</b>

2. S. Seok, "Polymer-based biocompatible packaging for implantable devices: packaging method, materials, and reliability simulation," *Micromachines* **12**, 1020 (2021).
3. ZEISS, "Products," <https://www.zeiss.com.cn/corporate/home.html>.
4. KEYENCE, "Products," <https://www.keyence.com.cn/products/>.
5. Y. Yu, D. L. Lau, M. P. Ruffner, and K. Liu, "Dual-projector structured light 3D shape measurement," *Appl. Opt.* **59**, 964–974 (2020).
6. F. Ren, Z. Wang, J. Qian, Y. Liang, S. Dang, Y. Cai, P. R. Bianco, B. Yao, and M. Lei, "Multi-view object topography measurement with optical sectioning structured illumination microscopy," *Appl. Opt.* **58**, 6288–6294 (2019).
7. Z. Zhu, C. Yang, H. Zhang, F. Zhang, and X. Liu, "Use of color information for structured-light 3D shape measurement of objects with shiny surfaces," *Appl. Opt.* **59**, 6873–6880 (2020).
8. A.-H. Nguyen, K. L. Ly, C. Q. Li, and Z. Wang, "Single-shot 3D shape acquisition using a learning-based structured-light technique," *Appl. Opt.* **61**, 8589–8599 (2022).
9. Q. Cui and R. Liang, "Chromatic confocal microscopy using liquid crystal display panels," *Appl. Opt.* **58**, 2085–2090 (2019).
10. S. Li and R. Liang, "DMD-based three-dimensional chromatic confocal microscopy," *Appl. Opt.* **59**, 4349–4356 (2020).
11. Y. Masaki, K. Tomita, Y. Kojima, and F. Kannari, "Measurement of propagation of ultrafast surface plasmon polariton pulses using dual-probe scanning near-field optical microscopy," *Appl. Opt.* **58**, 5595–5601 (2019).
12. H. Altamar-Mercado, A. Patiño-Vanegas, and A. G. Marrugo, "Robust 3D surface recovery by applying a focus criterion in white light scanning interference microscopy," *Appl. Opt.* **58**, A101–A111 (2019).
13. R.-Y. Yuan, X.-L. Ma, Y. Zheng, Z. Jiang, X. Wang, C. Liu, and Q.-H. Wang, "3D microscope image acquisition method based on zoom objective," *Opt. Express* **31**, 16067–16080 (2023).
14. C. Liu, Z. Jiang, X. Wang, Y. Zheng, Y.-W. Zheng, and Q.-H. Wang, "Continuous optical zoom microscope with extended depth of field and 3D reconstruction," *Photonix* **3**, 20 (2022).
15. A. Vasiman, J. R. Stothard, and I. I. Bogoch, "Mobile phone devices and handheld microscopes as diagnostic platforms for malaria and neglected tropical diseases (NTDs) in low-resource settings: a systematic review, historical perspective and future outlook," *Adv. Parasit.* **103**, 151–173 (2019).
16. J. Wang, Z. Zhen, Y. Wang, R. Wu, Y. Hu, Q. Fu, Y. Li, B. Xin, J. Song, J. Li, Y. Ren, L. Feng, H. Cheng, A. Wang, L. Hu, S. Ling, and Y. Li, "Non-invasive skin imaging assessment of human stress during head-down bed rest using a portable handheld two-photon microscope," *Front. Physiol.* **13**, 899830 (2022).
17. F. Cai, T. Wang, W. Lu, and X. Zhang, "High-resolution mobile bio-microscope with smartphone telephoto camera lens," *Optik* **207**, 164449 (2020).
18. D. Rabha, M. A. Rather, M. Mandal, and P. Nath, "Programmable illumination smartphone microscopy (PISM): a multimodal imaging platform for biomedical applications," *Opt. Laser Eng.* **151**, 106931 (2022).
19. P. Gordon, V. P. Venancio, S. U. Mertens-Talcott, and G. Coté, "Portable bright-field, fluorescence, and cross-polarized microscope toward point-of-care imaging diagnostics," *J. Biomed. Opt.* **24**, 1 (2019).
20. Y. Bian, Y. Jiang, Y. Huang, X. Yang, W. Deng, H. Shen, R. Shen, and C. Kuang, "Smart-phone phase contrast microscope with a singlet lens and deep learning," *Opt. Laser Technol.* **139**, 106900 (2021).
21. H. Tobon-Maya, S. Zapata-Valencia, E. Zora-Guzmán, C. Buitrago-Duque, and J. Garcia-Sucerquia, "Open-source, cost-effective, portable, 3D-printed digital lensless holographic microscope," *Appl. Opt.* **60**, A205–A214 (2021).
22. S. Dong, K. Guo, P. Nanda, R. Shiradkar, and G. Zheng, "FPscope: a field-portable high-resolution microscope using a cellphone lens," *Biomed. Opt. Express* **5**, 3305 (2014).
23. HUAWEI, "Support," <https://www.huawei.com/ca/>.
24. M. Zajac and J. Nowak, "Hybrid triplet objective with optimum aberration correction," *Optik* **118**, 115–119 (2007).
25. Z. Zhang and R. Lu, "Initial structure of dispersion objective for chromatic confocal sensor based on doublet lens," *Opt. Laser Eng.* **139**, 106424 (2021).
26. Daheng Imaging, "Products," [https://www.daheng-imaging.com/?bd\\_vid=11860249845986469382](https://www.daheng-imaging.com/?bd_vid=11860249845986469382).
27. H. Yang and G. Xue, "Products," <https://www.hengyangbuy.com/>.
28. L. Galdón, J. Garcia-Sucerquia, G. Saavedra, M. Martínez-Corral, and E. Sánchez-Ortiga, "Resolution limit in opto-digital systems revisited," *Opt. Express* **31**, 2000–2012 (2023).
29. Wibox, "Three-M," <https://www.wibox.net/>.
30. C. Wu, "VisualSFM: a visual structure from motion system," <http://ccwu.me/vsfm/>.
31. MeshLab, "Mister P. YouTube tutorials," <http://meshlab.sourceforge.net/>.
32. Phenix, "Products," <https://www.phenixoptics.com.cn/#>.
33. Computar, "Lenses," <https://computar.com/>.